Grp78 Heterozygosity Promotes Adaptive Unfolded Protein Response and Attenuates Diet-Induced Obesity and Insulin Resistance

Risheng Ye,[1] Dae Young Jung,[2] John Y. Jun,[2] Jianze Li,[1] Shengzhan Luo,[1] Hwi Jin Ko,[2] Jason K. Kim,[2] and Amy S. Lee[1]

OBJECTIVE—To investigate the role of the endoplasmic reticulum (ER) chaperone glucose-regulated protein (GRP) 78/BiP in the pathogenesis of obesity, insulin resistance, and type 2 diabetes.

RESEARCH DESIGN AND METHODS—Male *Grp78*$^{+/-}$ mice and their wild-type littermates were subjected to a high-fat diet (HFD) regimen. Pathogenesis of obesity and type 2 diabetes was examined by multiple approaches of metabolic phenotyping. Tissue-specific insulin sensitivity was analyzed by hyperinsulinemic-euglycemic clamps. Molecular mechanism was explored via immunoblotting and tissue culture manipulation.

RESULTS—*Grp78* heterozygosity increases energy expenditure and attenuates HFD-induced obesity. *Grp78*$^{+/-}$ mice are resistant to diet-induced hyperinsulinemia, liver steatosis, white adipose tissue (WAT) inflammation, and hyperglycemia. Hyperinsulinemic-euglycemic clamp studies revealed that *Grp78* heterozygosity improves glucose metabolism independent of adiposity and following an HFD increases insulin sensitivity predominantly in WAT. As mechanistic explanations, *Grp78* heterozygosity in WAT under HFD stress promotes adaptive unfolded protein response (UPR), attenuates translational block, and upregulates ER degradation-enhancing α-mannosidase–like protein (EDEM) and ER chaperones, thus improving ER quality control and folding capacity. Further, overexpression of the active form of ATF6 induces protective UPR and improves insulin signaling upon ER stress.

CONCLUSIONS—HFD-induced obesity and type 2 diabetes are improved in *Grp78*$^{+/-}$ mice. Adaptive UPR in WAT could contribute to this improvement, linking ER homeostasis to energy balance and glucose metabolism. ***Diabetes*** **59:6–16, 2010**

From the [1]Department of Biochemistry and Molecular Biology, University of Southern California/Norris Comprehensive Cancer Center, University of Southern California Keck School of Medicine, Los Angeles, California; and the [2]Department of Cellular and Molecular Physiology, Pennsylvania State University College of Medicine, Hershey, Pennsylvania.

D.Y.J., H.J.K., and J.K.K. are currently affiliated with the Department of Molecular Medicine, University of Massachusetts Medical School, Worcester, Massachusetts. S.L. is currently affiliated with the Department of Biological Sciences, Stanford University, Stanford, California.

Corresponding author: Amy S. Lee, amylee@ccnt.usc.edu.

Received 19 May 2009 and accepted 9 September 2009. Published ahead of print at http://diabetes.diabetesjournals.org on 6 October 2009. DOI: 10.2337/db09-0755.

The endoplasmic reticulum (ER) is a specialized perinuclear organelle where secretory and membrane proteins, as well as lipids, are synthesized. It is also a major intracellular storage compartment for Ca^{2+}, which regulates multiple pathways of signal transduction. ER stress is defined as an imbalance between protein load and folding capacity of the ER, which triggers the evolutionarily conserved mechanism referred to as the unfolded protein response (UPR) (1). The UPR induces three major ER signaling pathways, namely PKR-like endoplasmic reticulum kinase (PERK), inositol requiring-1 (IRE-1), and activating transcription factor (ATF) 6. As an acute response, autophosphorylation of PERK leads to phosphorylation of eukaryotic initiation factor (eIF) 2α and global inhibition of mRNA translation, immediately reducing ER protein load. However, this early protective process is unfavorable for long-term cellular function and is reversible during the adaptive phase of UPR. The adaptive UPR signaling, including activation of transcription factors ATF4 (by eIF2α phosphorylation), X-box binding protein (XBP)-1 (by active IRE-1), and ATF6, promotes recovery from translational block, ER-associated protein degradation (ERAD), and upregulation of ER chaperones (2). Within the lumen of the ER, protein chaperones and folding enzymes such as glucose-regulated protein (GRP)78, GRP94, protein disulphide isomerase (PDI), calnexin (CNX), and calreticulin (CRT) assist in folding of newly synthesized polypeptides and prevent aggregation of unfolded or misfolded protein (3). Differentiated adipocytes are potent endocrine cells, secreting large amounts of peptides and lipid mediators such as leptin and adiponectin (4). Biosynthesis of these adipokines requires chaperones and folding enzymes in the ER. Thus, ER stress of adipocytes may play a significant role in obesity-related pathogenesis, and understanding the contribution of the UPR to adipocyte stress may identify new targets toward the development of preventive and therapeutic strategies (5).

The molecular mechanism linking obesity to insulin resistance in the peripheral tissues has recently been elucidated in mouse models (6). Excessive fat storage stimulates ER stress in liver and adipose tissue, which subsequently activates IRE-1 and the downstream kinase, c-Jun NH_2-terminal kinase (JNK), through the ER stress signaling pathway. Active JNK can phosphorylate the insulin receptor substrate (IRS)-1 on Ser307, thus inhibiting tyrosine phosphorylation of IRS-1 and the downstream insulin signaling pathway (7). Administration of chemical chaperones such as 4-phenyl butyric acid or tauroursodeoxycholic acid was able to reduce ER stress, restore

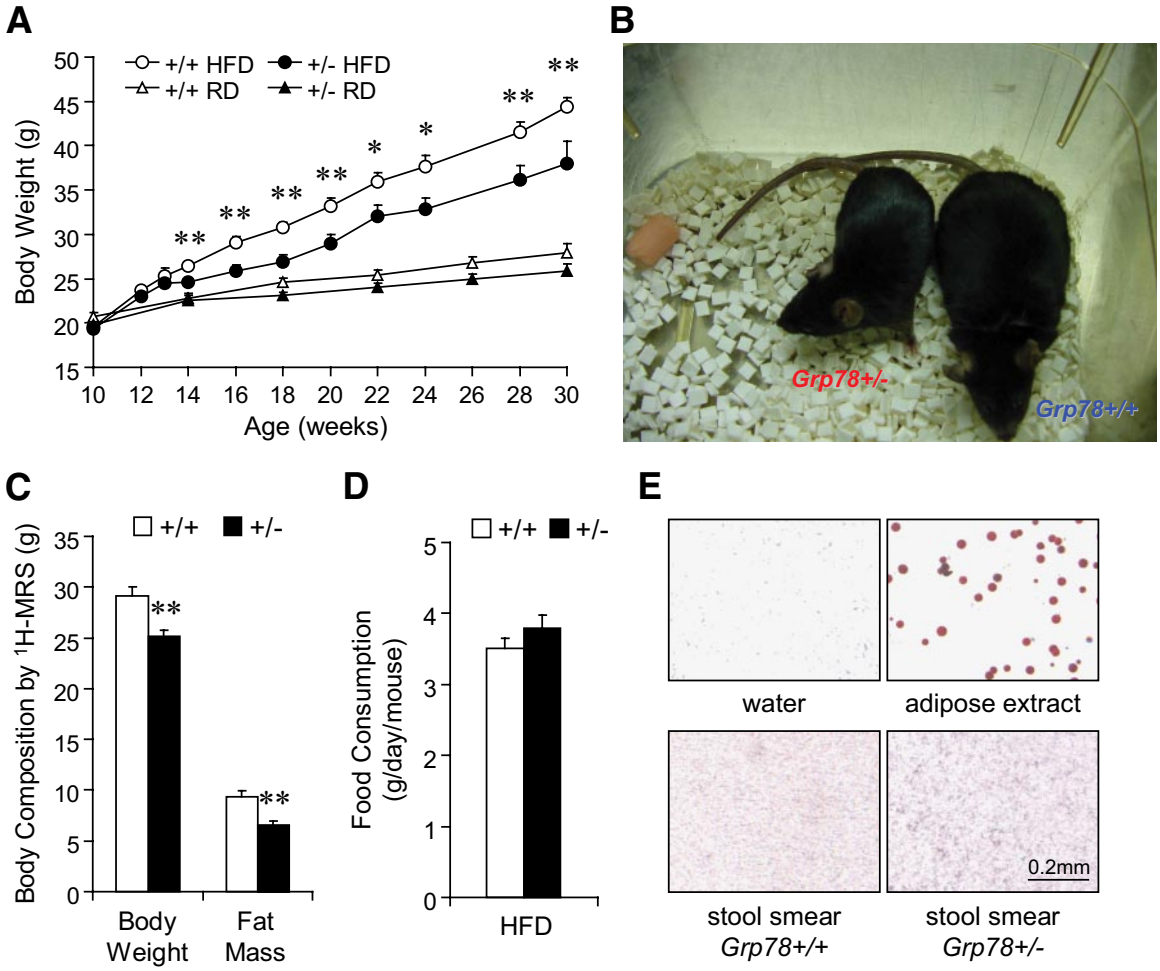

FIG. 1. Attenuation of diet-induced obesity in *Grp78*$^{+/-}$ mice. *A*: Fasting body weight on regular diet (RD) or HFD from 10-week-old mice ($n \geq 7$ mice per condition). ○, $^{+/+}$ HFD; ●, $^{+/-}$ HFD; △, $^{+/+}$ regular diet; ▲, $^{+/-}$ regular diet. *B*: Body size after 20-week HFD. *C*: Body composition after 11-week HFD. $n = 9$ ($^{+/+}$, □) or 6 ($^{+/-}$, ■). *D*: Food intake measurement. $n = 7$ ($^{+/+}$, □) or 5 ($^{+/-}$, ■). *E*: Oil Red O staining of stool smear from mice on HFD. Negative control: dH_2O; positive control: white adipose extract. Data are presented as the means ± SE. *$P < 0.05$; **$P < 0.01$ for $^{+/-}$ vs. $^{+/+}$. (A high-quality color digital representation of this figure is available in the online issue.)

glucose homeostasis, and improve insulin sensitivity in the peripheral tissues of leptin-deficient *ob/ob* mice (8), implying that ER homeostasis is key to improved glucose tolerance.

The 78-kDa glucose regulated protein GRP78, also referred to as BiP (immunoglobulin heavy-chain binding protein) or HSPA5, is a key rheostat in controlling ER homeostasis. GRP78 regulates ER function due to its role in protein folding and assembly, targeting misfolded protein for degradation, ER Ca^{2+} binding, and controlling the activation of transmembrane ER stress sensors (3,9,10). Among the peripheral tissues, GRP78 expression is readily detected in adult adipose tissues and liver but is very low in muscle. To study its in vivo role in cell metabolism, we created targeted mutation of the *Grp78* allele in mouse models. Homozygous deletion of *Grp78* results in early embryonic lethality; however, the *Grp78*$^{+/-}$ mice with partial reduction in GRP78 expression level are viable and fertile (11). Serendipitously, we discovered that the *Grp78*$^{+/-}$ mice in the C57BL/6 genetic background substantially mitigates high-fat diet (HFD)-induced obesity and insulin resistance. In addition to improved energy expenditure, a striking increase in insulin-stimulated glucose uptake was observed in the white adipose tissue (WAT) of *Grp78*$^{+/-}$ mice. We further discovered that *Grp78* heterozygosity in WAT triggers adaptive UPR signaling as well as compensatory increases in ER chaperone levels, associating with attenuation of translational block and improved insulin signaling. As proof of principle, overexpression of active ATF6 in mouse embryo fibroblasts (MEFs) induces protective UPR and leads to improvement of insulin sensitivity under ER stress. Thus, the *Grp78*$^{+/-}$ mouse model uncovers novel modulatory mechanisms in WAT linking ER integrity to energy balance, glucose homeostasis, and adipocyte stress.

RESEARCH DESIGN AND METHODS

The *Grp78*$^{+/-}$ mice were generated as described (11) and were backcrossed into the C57BL/6 genetic background for five to eight generations. Mice were fed on regular diet (11% fat by calories; Harlan Teklad) continuously after weaning (at ~3 weeks of age) or changed to HFD (45% fat by calories; Research Diets) at 10 weeks of age. Only male mice were used in this study. Mouse body weight was measured after overnight fasting. Food intake was analyzed by daily food mass measurement for 5 successive days during the third week of the HFD regimen. Mouse stool was processed to Oil-O-Red staining for lipids as described (12). All protocols for animal use and euthanasia were reviewed and approved by the University of Southern California Institutional Animal Care and Use Committee.

Measurement of body composition and energy balance. Twenty-week-old mice were fed an HFD for 10 weeks. Whole-body fat and lean mass were noninvasively measured in conscious mice using proton magnetic resonance

spectroscopy (^{1}H-MRS) (Echo Medical Systems, Houston, TX). A 3-day measurement of water intake, energy expenditure, and physical activity was performed using the metabolic cages (TSE Systems, Bad Homburg, Germany). All procedures were approved by the Pennsylvania State University Institutional Animal Care and Use Committee.

Assay of blood glucose and insulin. Mouse tail blood was measured for glucose by the OneTouch Ultra System (LifeScan, Milpitas, CA). For insulin, plasma was prepared from blood by centrifugation and measured with an enzyme-linked immunosorbent assay (ELISA) kit (Linco Research).

Tissue processing. After the mice were killed, mouse tissues were fixed in 10% formalin for histological analysis or immediately frozen in liquid nitrogen and stored at −80°C for immunoblotting.

Immunohistochemistry. Paraffin sections of formalin-fixed tissues were stained with hematoxylin and eosin for morphological evaluation. For immunohistochemistry, primary antibodies used included insulin (1:100; Signet) and CD68 (1:50; Santa Cruz Biotechnology).

Insulin tolerance test. Mice were subjected to intraperitoneal injection of insulin (0.5 mU/g body wt) after 6 h fasting, followed by blood glucose measurement.

Hyperinsulinemic-euglycemic clamp. After a 10-week HFD regimen, 20-week-old mice were subjected to hyperinsulinemic-euglycemic clamp to assess insulin sensitivity in vivo as described (13). Details of the clamp methodology, biochemical assays, and the metabolic rate calculations were described in online appendix (available at http://diabetes.diabetesjournals.org/cgi/content/full/db09-0755/DC1).

Insulin signaling analysis. Following clamps, WAT was prepared for lysates. Total and phospho-Tyr IRS-1 levels were analyzed by immunoblotting. Insulin-stimulated AKT activity was determined by immunoprecipitating tissue lysates with a polyclonal AKT antibody (Upstate Biotechnology) that recognized both AKT1 and AKT2, coupled with protein G–Sepharose beads (Amersham Pharmacia Biotechnology, Piscataway, NJ) as previously described (13).

Cell culture and transfection. The *Grp78*$^{+/-}$ MEFs were isolated and immortalized with SV40 large-tumor antigen as described (14). The similarly transformed wild-type MEFs were provided by Dr. Stanley Korsmeyer (Harvard University). To overexpress an HA-tagged active nuclear form of ATF6, cells were transfected with the plasmid pCGN-ATF6(373) (15) using PolyFect (Qiagen) for 24 h, controlled by the vector transfection. To induce ER stress, cells were treated with tunicamycin (1.5 μg/ml; Sigma) for 14 h.

Insulin sensitivity analysis. After cultured in serum-free medium for 5 h, cells were treated with insulin (100 nmol/l; Sigma) for 15 min, followed by immediate lysate preparation (16). Insulin-stimulated phosphorylation of AKT was determined by immunoblotting phosphor-Ser473 and total AKT.

Immunoblotting. Lysates of tissues from individual mice or cells were extracted in ice-cold radioimmunoprecipitation assay buffer (50 mmol/l Tris-Cl, 150 mmol/l NaCl, 1% NP-40, 0.5% sodium deoxycholate, and 0.1% SDS), containing cocktails of proteinase inhibitors and phosphatase inhibitors (Roche), by centrifugation (13,000*g*, 15 min) following homogenization and three freeze-thaw cycles. Proteins were separated by 8% or 12% SDS-PAGE and transferred to nitrocellulose membrane (Pall) and subjected to Western blotting (15). Primary antibodies used included pSer473-AKT, AKT (1:1,000; Cell Signaling or Upstate Biotechnology), pTyr–IRS-1, IRS-1 (Upstate Biotechnology), JNK1, glyceraldehyde-3-phosphate dehydrogenase, ATF4, CHOP, GADD34, XBP-1, ER degradation-enhancing α-mannosidase-like protein (EDEM), GRP78, hemagglutinin (HA) tag (1:1,000; Santa Cruz Biotechnology), pSer51-eIF2α, eIF2α (1:1,000; Cell Signaling), ATF6 (1:100; Abcam), GRP94, PDI, CNX, and CRT (1:2000; Stressgen), peroxisome proliferator–activated receptor γ coactivator (PGC)-1 (1:1,000, Calbiochem), and β-actin (1:5,000; Sigma). Western blotting was repeated two to six times and quantitated using the Quantity One system (Bio-Rad).

Statistical analysis. A two-tailed Student's *t* test was applied for all pairwise comparisons.

RESULTS

***Grp78* heterozygosity increases energy expenditure and attenuates diet-induced obesity.** To investigate the role of GRP78 in obesity and type 2 diabetes, cohorts of *Grp78*$^{+/-}$ mice and their wild-type ($^{+/+}$ mice, *Grp78*$^{+/+}$) littermates in a C57BL/6 background were subjected to the HFD regimen beginning at the age of 10 weeks. Male mice were used since hormonal cycle in females may affect metabolism and confound the results. Surprisingly, we discovered that following HFD, *Grp78*$^{+/-}$ mice showed significantly lower body weight than the $^{+/+}$ siblings (Fig. 1*A* and *B*), as confirmed by body composition analysis by

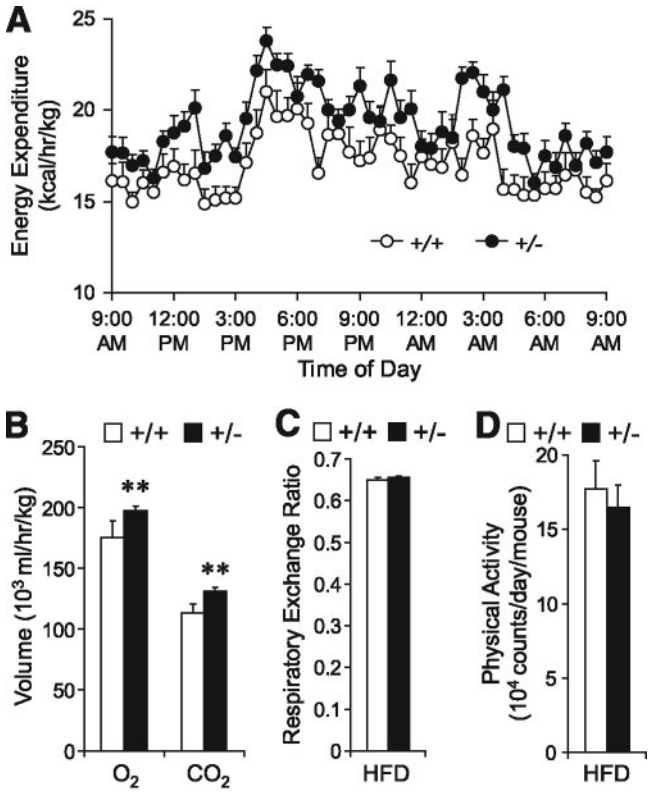

FIG. 2. Enhancement of energy expenditure in *Grp78*$^{+/-}$ mice. Metabolic cage studies on mice after 10-week HFD ($n \geq 3$ mice per condition). *A*: Energy expenditure. *B*: O_2 consumption and CO_2 production. *C*: Respiratory exchange ratio. *D*: Total physical activity. Data are presented as the means ± SE. **$P < 0.01$ for $^{+/-}$ (■) vs. $^{+/+}$ (□).

^{1}H-MRS showing primarily reduction in fat mass (Fig. 1*C* and supplementary Fig. 1*A*). The lean phenotype of the *Grp78*$^{+/-}$ mice was not caused by alterations in food and water intake (Fig. 1*D* and supplementary Fig. 1*B*) or intestinal fat absorption (Fig. 1*E*). Rather, it is at least in part due to increased energy expenditure in the *Grp78*$^{+/-}$ mice, as measured by indirect calorimetry (Fig. 2*A*). Significant enhancement of both O_2 consumption ($P = 0.006$) and CO_2 production ($P = 0.0009$) was observed in the $^{+/-}$ mice (Fig. 2*B*). In contrast, no difference was observed in the respiratory exchange ratios (Fig. 2*C*) or physical activities (Fig. 2*D*).

***Grp78*$^{+/-}$ mice are resistant to diet-induced hyperinsulinemia, liver steatosis, WAT inflammation, and hyperglycemia.** Diet-induced obesity causes insulin resistance, pancreatic islet hyperplasia, hyperinsulinemia, and hyperglycemia (17). After 20 weeks of HFD (30 weeks old), while $^{+/+}$ mice developed hyperglycemia (159 ± 6 mg/dl) as expected, $^{+/-}$ mice maintained significantly lower fasting glucose level (118 ± 9 mg/dl) (Fig. 3*A*). The fasting plasma insulin level was also lower in the $^{+/-}$ mice (0.26 ± 0.06 vs. 0.55 ± 0.08 ng/ml in $^{+/+}$ mice, $P = 0.009$) (Fig. 3*B*). The $^{+/-}$ mice were resistant to HFD-induced β-cell hyperplasia evident in the $^{+/+}$ mice (Fig. 3*C*), contrasting with normal glucagon distribution staining pattern for both $^{+/+}$ and $^{+/-}$ mice (supplementary Fig. 2*A*). Transmission electron microscopy further showed that $^{+/-}$ pancreatic β-cells had normal number and distribution of secretory granules (supplementary Fig. 2*B*). Hepatic steatosis could be a complication of diet-induced type 2 diabetes (18). In agreement with the improved hypergly-

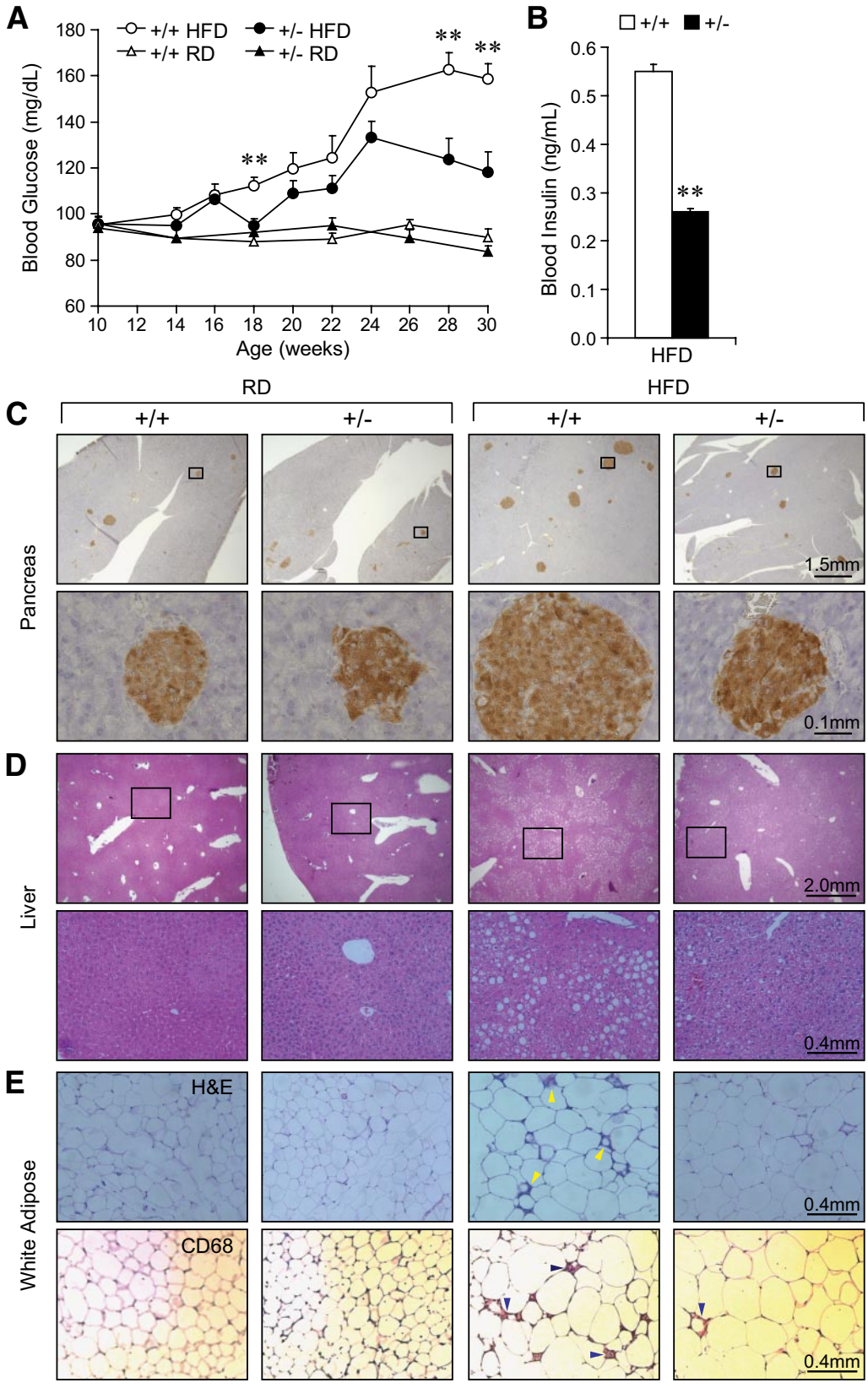

FIG. 3. Resistance to HFD-induced diabetic phenotypes in *Grp78*$^{+/-}$ mice. *A*: Fasting blood glucose ($n \geq 7$ mice per condition). ○, $^{+/+}$ HFD; ●, $^{+/-}$ HFD; △, $^{+/+}$ regular diet; ▲, $^{+/-}$ regular diet. *B*: Fasting blood insulin after 19-week HFD. $n = 15$ ($^{+/+}$, □) or 16 ($^{+/-}$, ■). Data are presented as means ± SE. **$P < 0.01$ for $^{+/-}$ vs. $^{+/+}$. *C–E*: Histochemical studies on 25-week-old mice on regular diet (RD) or after 15-week HFD ($n \geq 3$ mice per condition). Numbers above scale bars indicate the represented object distance. *C*: Insulin immunostaining on pancreas. *D*: Hematoxylin and eosin staining on liver (*C* and *D*: *Lower panels* exhibit the boxed areas within the corresponding *upper panels*.) *E*: Hematoxylin and eosin and CD68 staining on WAT. Arrowheads indicate inflammation. (A high-quality color digital representation of this figure is available in the online issue.)

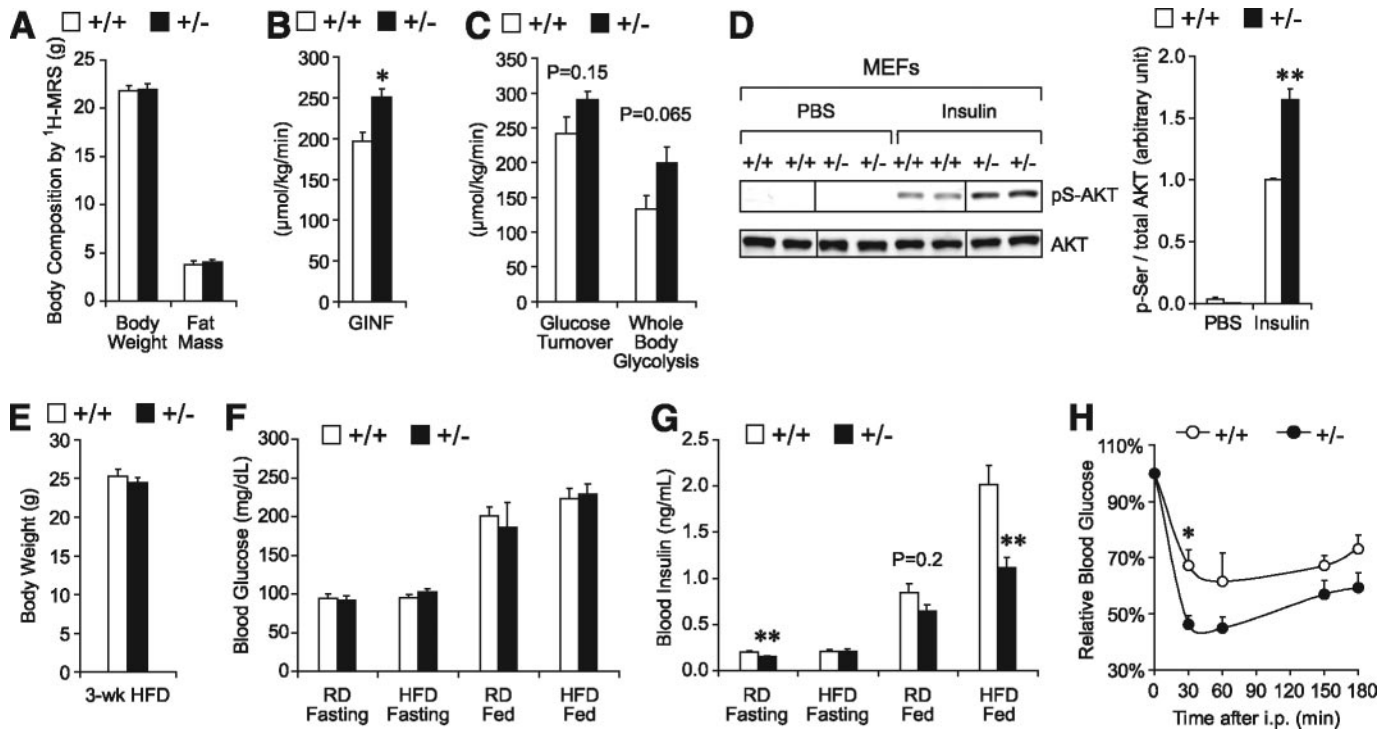

FIG. 4. *Grp78* heterozygosity improves insulin sensitivity independently of adiposity. *A–C*: Hyperinsulinemic-euglycemic clamp studies on 13-week-old $^{+/+}$ ($n = 5$) and $^{+/-}$ ($n = 4$) mice on regular diet (RD). *A*: Body composition. *B*: GINF. *C*: Whole-body glucose turnover and glycolysis during clamps. *D*: Immortalized *Grp78*$^{+/-}$ and $^{+/+}$ MEFs were treated with insulin (100 nmol/l, 15 min) following 5-h serum starvation. Whole cell lysates were subjected to Western blot for phosphorylated (Ser473) and total AKT. Lanes were run on the same gel but noncontiguous. *E–H*: For 13-week-old mice on regular diet or after 3-week HFD. *E*: Fasting body weight (HFD). *F*: Blood glucose (regular diet and HFD). *G*: Blood insulin (regular diet and HFD). (*E–G*: $n \geq 6$ mice per condition.) *H*: Insulin tolerance test (HFD). $n = 4$ ($^{+/+}$, ○) or 5 ($^{+/-}$, ●). Data are presented as the means ± SE. *$P < 0.05$; **$P < 0.01$ for $^{+/-}$ vs. $^{+/+}$. □, $^{+/+}$; ■, $^{+/-}$.

cemia (Fig. 3*A*), the $^{+/-}$ mice showed reduced steatosis in liver (Fig. 3*D*). Adipose inflammation has recently been linked to obesity-associated insulin resistance (19). Correspondingly, WAT from the $^{+/-}$ mice showed greatly reduced inflammation, as revealed by hematoxylin and eosin and CD68 staining (Fig. 3*E*). Compared with the regular diet–fed mice, the HFD regimen led to an increase in adipocyte size in both *Grp78*$^{+/+}$ and $^{+/-}$ mice. However, there is no apparent difference in adipocyte size or morphology between the two genotypes, either regular diet fed or HFD fed (Fig. 3*E*).

***Grp78* heterozygosity improves glucose metabolism independent of adiposity.** To test whether *Grp78* heterozygosity–mediated improvement on glucose metabolism is dependent on adiposity, we performed a hyperinsulinemic-euglycemic clamp on regular diet–fed mice at the age of 13 weeks, when there was no significant difference in body weight and fat mass between the two genotypes (Fig. 4*A*). Steady-state glucose infusion rates (GINF) to maintain euglycemia were significantly elevated in the $^{+/-}$ mice, corresponding with increased insulin sensitivity (Fig. 4*B*). Insulin-stimulated whole-body glucose turnover and glycolysis both exhibited a trend toward enhancement in the $^{+/-}$ mice (Fig. 4*C*). These data suggest that *Grp78* heterozygosity improves glucose metabolism and insulin sensitivity in mice, independent of reduced adiposity. As supporting evidence, we established MEF cell lines from *Grp78*$^{+/+}$ and $^{+/-}$ mice and subjected them to insulin stimulation following serum starvation in culture. We observed increase of insulin-stimulated AKT phosphorylation in *Grp78*$^{+/-}$ MEFs compared with wild-type MEFs (1.6-fold, $P = 0.002$) (Fig. 4*D*). Thus, *Grp78* heterozygosity improves insulin sensitivity in MEFs in culture.

Toward further confirmation, we examined metabolic parameters after 3 weeks of HFD when the body weights were comparable between the $^{+/-}$ and $^{+/+}$ mice (Fig. 4*E*). While both $^{+/+}$ and $^{+/-}$ mice were able to maintain normal blood glucose levels at both fasting and fed states (Fig. 4*F*), HFD-fed $^{+/-}$ mice exhibited a 45% decrease in fed insulin level (1.12 ± 0.11 vs. 2.01 ± 0.21 ng/ml in $^{+/+}$ mice, $P = 0.002$) (Fig. 4*G*). In addition, blood insulin level was decreased ~25% in the age-matched 13-week-old regular diet–fed $^{+/-}$ mice, at both fasting ($P = 0.008$) and fed ($P = 0.2$) states (Fig. 4*G*), consistent with the clamp studies (Fig. 4*B* and *C*). This decrease was magnified by the HFD challenge, since an insulin tolerance test performed at 3 weeks of HFD showed improved glucose clearance for the $^{+/-}$ mice (Fig. 4*H*). Collectively, the results show that *Grp78* heterozygosity enhances insulin sensitivity in both in vivo and in vitro systems.

***Grp78*$^{+/-}$ mice fed on HFD exhibit a striking increase in insulin sensitivity in WAT.** Toward understanding how the HFD-fed *Grp78*$^{+/-}$ mice improve glucose metabolism, a hyperinsulinemic-euglycemic clamp was performed after 10–11 weeks of HFD to examine the insulin sensitivity of individual tissues (Fig. 5*A–E*). Whole-body glucose metabolism was significantly elevated in the $^{+/-}$ mice, both at steady state and upon insulin stimulation, corresponding with increased insulin sensitivity (Fig. 5*A*). Insulin-stimulated whole-body glucose flux (glycolysis and glycogen plus lipid synthesis) was increased by ~25% in the $^{+/-}$ mice (Fig. 5*B*). Organ-specific glucose metabolism was assessed using 2-deoxy-D-[1-^{14}C]glucose injection during clamps. Strikingly, for the $^{+/-}$ mice, insulin-stimulated glucose uptake was increased by twofold in WAT ($P = 0.001$) (Fig. 5*C*) but was unaltered in skeletal muscle and

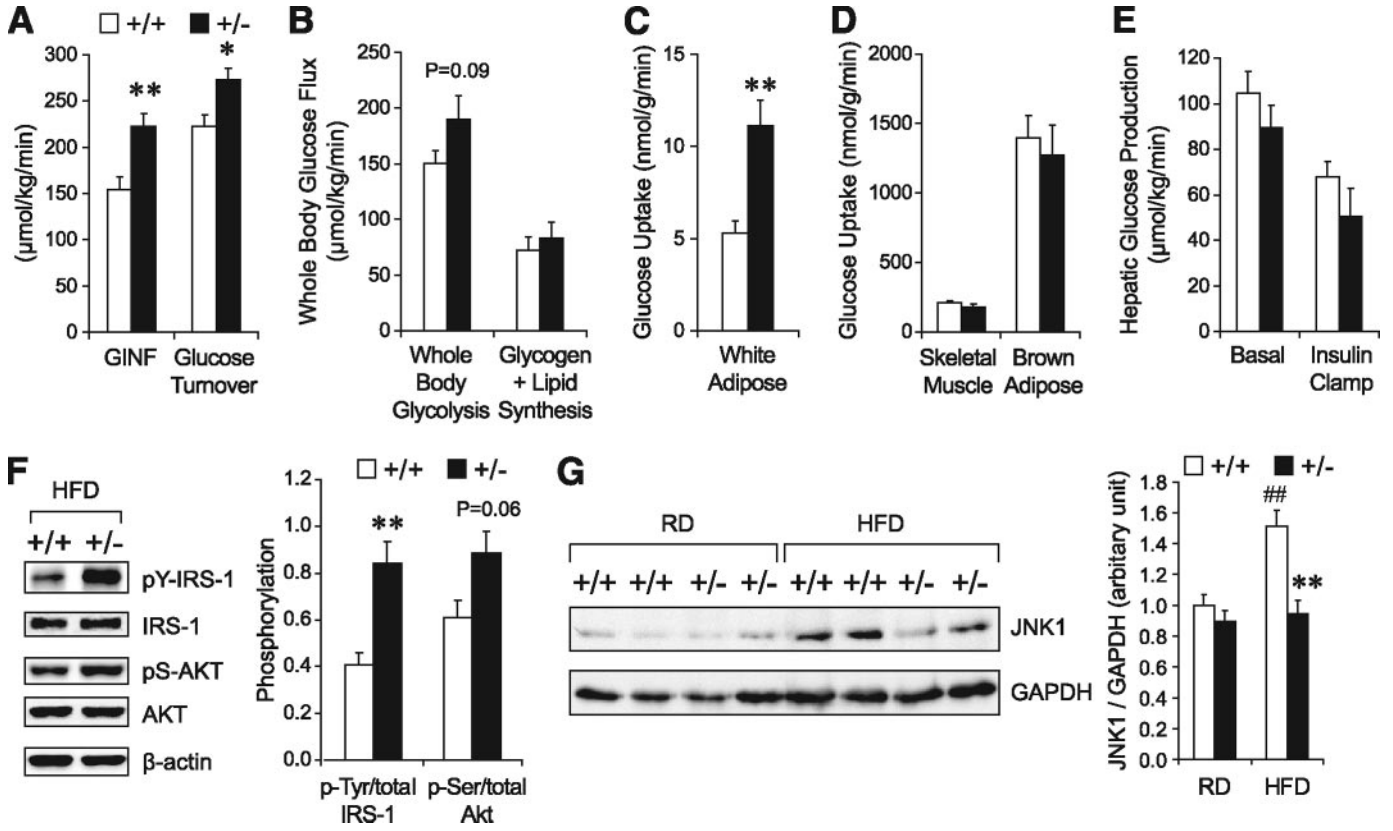

FIG. 5. *Grp78* heterozygosity improves insulin sensitivity predominantly in WAT. *A–E*: Hyperinsulinemic-euglycemic clamp studies on $^{+/-}$ (■, n = 6) and $^{+/+}$ (□, n = 9) mice after 10–11 weeks of HFD. *A*: Whole-body glucose metabolism indicated by GINF and clamp glucose turnover. *B*: Whole-body glycolysis and glucose anabolism during clamps. *C* and *D*: Glucose uptake by white adipose (*C*), skeletal muscle, and brown adipose (*D*) during clamps. *E*: Hepatic glucose production. *F* and *G*: Representative Western blots and quantitation of phosphorylation of IRS-1 (Tyr) and AKT (Ser473) in WAT of mice after clamps (n = 4 mice per genotype) (*F*) and JNK1 in WAT of 25-week-old mice on regular diet (RD) or after 15-week HFD (n = 3–5 mice per condition) (*G*). □, $^{+/+}$; ■, $^{+/-}$. Data are presented as the means ± SE. *P < 0.05; **P < 0.01 for $^{+/-}$ vs. $^{+/+}$; ##P < 0.01 for HFD vs. regular diet.

brown adipose tissue (Fig. 5*D*). There was a trend toward increased insulin sensitivity in $^{+/-}$ liver, indicated by a lower rate of hepatic glucose production at basal and clamp states (Fig. 5*E*). We further observed increases in insulin-stimulated phosphorylation of IRS-1 (2.1-fold, P = 0.006) and AKT (1.5-fold, P = 0.06) in the WAT of the $^{+/-}$ mice (Fig. 5*F*), suggesting that *Grp78* heterozygosity improves IRS-associated insulin signaling. JNK1 was reported to be upregulated by obesity and to impair insulin signaling (6,7). A 38% decrease (P = 0.004) in JNK1 level was observed in the WAT of the $^{+/-}$ mice on HFD, compared with the HFD-fed $^{+/+}$ mice (Fig. 5*G*). This is consistent with the improved insulin signaling that resulted from *Grp78* heterozygosity and the recent findings that JNK1 deletion in adipose tissue increased AKT signaling in HFD-fed mice (20).

***Grp78* heterozygosity promotes adaptive UPR and improves ER homeostasis in WAT.** Considering that GRP78 is well established to protect against ER stress, which activates inflammation and inhibits insulin signaling in both genetic and diet-induced obese mouse models (6), it is unanticipated that *Grp78* heterozygosity confers beneficial metabolic effects. However, chronic ER stress could elicit adaptive survival responses that improve protein folding capacity of the ER, while destabilizing the proapoptotic pathways (21). Partial loss of GRP78 due to *Grp78* heterozygosity could mimic low chronic ER stress and promote adaptive UPR. To test this, protein lysates were prepared from WAT of *Grp78*$^{+/+}$ and $^{+/-}$ mice and the UPR signaling molecules and their downstream targets were examined by Western blot (supplementary Fig. 3) and the expression levels were quantitated and summarized (Fig. 6*A*). The level of Ser51 phosphorylation of the eukaryotic translation initiation factor eIF2α is a marker of ER stress and attenuation of global protein translation (22). In agreement with previous reports that HFD induces ER stress (6), eIF2α phosphorylation was dramatically increased in WAT of HFD-fed $^{+/+}$ mice (2.8-fold, P = 0.002), in comparison with the regular diet–fed $^{+/+}$ mice (Fig. 6*A*). The regular diet–fed $^{+/-}$ mice showed no significant elevation of eIF2α phosphorylation, but a 40% decrease was observed in HFD-fed $^{+/-}$ mice, compared with the HFD-fed $^{+/+}$ mice (P = 0.03).

How might *Grp78* heterozygosity reduce diet-induced eIF2α phosphorylation? As downstream signaling of eIF2α phosphorylation, upregulation of GADD34 by transcription factors ATF4 and CHOP mediates dominant dephosphorylation of eIF2α, thus promoting protein synthesis resumption and recovery from ER stress (23,24). We observed that while HFD significantly reduced the expression level of ATF4 and GADD34 in WAT of the $^{+/+}$ mice, this suppression was not observed in the WAT of the $^{+/-}$ mice (Fig. 6*A*). Thus, the ability of the WAT of $^{+/-}$ mice to maintain expression of the dominant regulator GADD34 under HFD stress could contribute in part to the attenuated eIF2α phosphorylation observed.

The ATF6 and the IRE-1 branches of the UPR signaling were also analyzed in WAT. We detected an increase in the

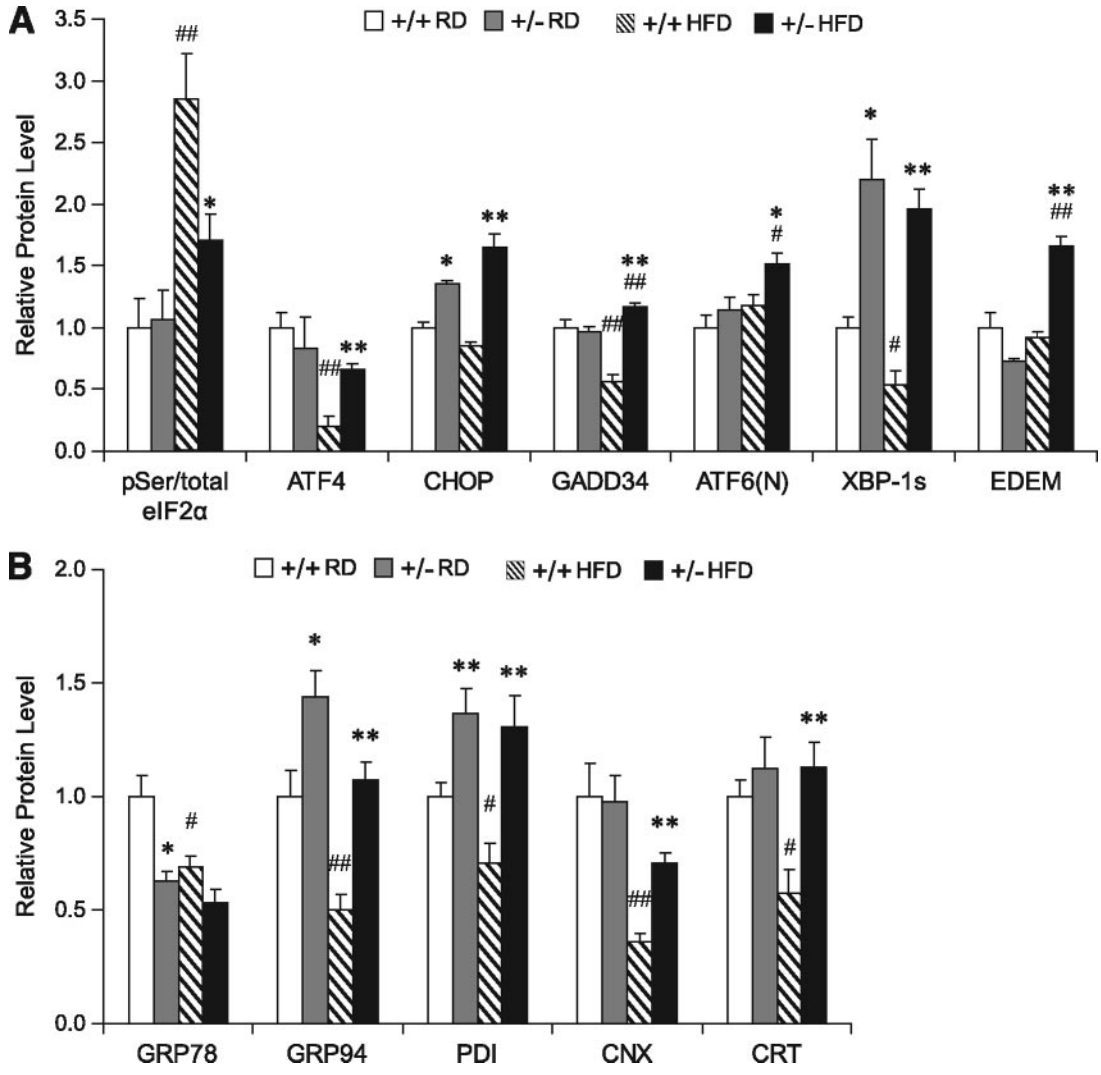

FIG. 6. *Grp78* heterozygosity promotes adaptive UPR and improves ER homeostasis in WAT. Whole cell lysates were prepared from WAT of 25-week-old mice on regular diet (RD) or after 15-week HFD (n = 4–6 mice per condition) and subjected to Western blotting. The protein loading was normalized against β-actin. Quantitation of relative protein levels of indicated UPR signaling molecules (*A*) and ER chaperones (*B*) are presented as the means ± SE. *P < 0.05; **P < 0.01 for $^{+/-}$ vs. $^{+/+}$; #P < 0.05; ##P < 0.01 for HFD vs. regular diet. □, $^{+/+}$ regular diet; ▨, $^{+/-}$ regular diet; ▧, $^{+/+}$ HFD; ■, $^{+/-}$ HFD.

active ATF6 cleaved form in WAT of HFD-fed $^{+/-}$ mice, compared with the $^{+/+}$ mice under both regular diet (1.5-fold, P = 0.003) and HFD (1.3-fold, P = 0.02) conditions and the $^{+/-}$ mice under regular diet (1.3-fold, P = 0.03) conditions (Fig. 6*A*). As an essential prosurvival transcription factor downstream of IRE-1 phosphorylation (2), spliced XBP-1 was strikingly elevated in $^{+/-}$ mice, either under regular diet–fed (2.2-fold, P = 0.02) or HFD-fed (3.6-fold, P = 0.002) conditions (Fig. 6*A* and supplementary Fig. 3). One of the protective roles of XBP-1 splicing during ER stress is to promote ERAD and improve protein quality control by transcriptional activation of a subset of genes, including EDEM (25). While the level of EDEM was relatively unchanged among regular diet–fed $^{+/+}$ or $^{+/-}$ mice, or HFD-fed $^{+/+}$ mice, consistently, a significant increase (1.8-fold, P = 0.001) of EDEM was observed in WAT of HFD-fed $^{+/-}$ mice in comparison to HFD-fed $^{+/+}$ mice (Fig. 6*A* and supplementary Fig. 3), suggesting that upon HFD stress, ERAD was induced in WAT by *Grp78* heterozygosity.

To monitor the ER protein folding capacity in WAT, the levels of ER chaperones GRP78, GRP94, PDI, CNX, and CRT, which are downstream targets of adaptive UPR, were measured by Western blot. As expected, heterozygous loss of the *Grp78* allele in the regular diet–fed $^{+/-}$ mice resulted in a partial decrease in GRP78 protein level (37%, P = 0.02) (Fig. 6*B*). On the other hand, GRP94 was increased by 1.4-fold (P = 0.03) and PDI by 1.4-fold (P = 0.009), and no change was detected for CNX and CRT levels (Fig. 6*B*). Similar observations were reported for primary *Grp78*$^{+/-}$ MEFs (11) and confirmed in the immortalized *Grp78*$^{+/-}$ MEF cell lines used in this study (supplementary Fig. 4*A*). Therefore, both in MEFs and WAT, *Grp78* heterozygosity induces compensatory upregulation of GRP94 and PDI in response to partial reduction of GRP78. Correspondingly, *Grp78*$^{+/-}$ MEF cell lines exhibited enhanced insulin sensitivity with or without tunicamycin-induced ER stress (supplementary Fig. 4*B*).

However, after 15 weeks of HFD, protein levels of GRP78, GRP94, PDI, CNX, and CRT were all significantly reduced (by ~30–65%) in the WAT of the $^{+/+}$ mice (Fig. 6*B*), despite increases in their mRNA levels (supplementary Fig. 5*A*), suggesting translational block or some other posttranscriptional regulation. To confirm this unantici-

pated finding, we expanded the observation on $^{+/+}$ mice after 3, 7, 10, or 24 weeks of HFD. Compared with the age-matched regular diet–fed $^{+/+}$ mice, protein levels of ER chaperones were significantly reduced in WAT after 10 weeks of the HFD regimen (supplementary Fig. 5*B*). Interestingly, for the HFD-fed $^{+/-}$ mice, GRP78 level was nearly comparable to the $^{+/+}$ mice, and all the other ER chaperone levels (GRP94, PDI, CNX, and CRT) were upregulated by about twofold compared with the HFD-fed $^{+/+}$ mice (Fig. 6*B*). These results suggest that HFD stress could decrease the ER protein folding capacity in the WAT of the $^{+/+}$ mice; however, *Grp78* heterozygosity promotes adaptive responses in WAT to maintain ER chaperone synthesis, which may contribute in part to the metabolic benefits. Consistent with this notion, in skeletal muscle of the $^{+/-}$ mice, where insulin sensitivity was not improved under HFD conditions (Fig. 5*D*), compensatory ER chaperone upregulation was not observed (supplementary Fig. 6*A*). In the $^{+/-}$ liver, showing a trend of enhanced insulin sensitivity after HFD (Fig. 5*E*), the level of GRP94, but not the other ER chaperones, was upregulated (supplementary Fig. 6*B*).

Recently, expression of metabolic genes was suggested to directly respond to ER homeostasis (26). Corresponding to the adaptive UPR and improved protein folding capacity in *Grp78*$^{+/-}$ WAT, we observed that the expression level of PGC-1α, a transcriptional coactivator and regulator of mitochondrial energy metabolism and biogenesis (27), was enhanced in the WAT of the regular diet–fed *Grp78*$^{+/-}$ mice (30% increase, $P = 0.03$) (Fig. 7*A*). Following 15 weeks of HFD, while the $^{+/+}$ mice showed a 74% decrease in PGC-1α level in WAT compared with the regular diet–fed $^{+/+}$ mice ($P = 0.00005$), the $^{+/-}$ mice showed a 90% increase compared with the HFD-fed $^{+/+}$ mice ($P = 0.004$) (Fig. 7*A*). Interestingly, GRP75, a mitochondrial chaperone mediating the coupling of ER and mitochondrial Ca^{2+} channels (28), was also upregulated in WAT of regular diet–fed (1.2-fold, $P = 0.02$) and HFD-fed (1.5-fold, $P = 0.008$) *Grp78*$^{+/-}$ mice (Fig. 7*B*).

As proof of principle that induction of protective UPR leads to improved insulin sensitivity under ER stress, we enforced expression of the active, nuclear form of ATF6 [ATF6(N)] in immortalized wild-type MEF cell line and tested for insulin sensitivity. The expression of HA-tagged ATF(N) was confirmed by Western blot in the transfected cells. Compared with cells transfected with the empty vector, cells expressing ATF(N) showed moderate upregulation of GRP94, GRP78, and CRT, and upon treatment of cells with ER stress inducer tunicamycin for 14 h, the overall level of these chaperones was further enhanced (Fig. 8*A*).

Insulin sensitivity of the cells was monitored by Ser473 phosphorylation of AKT upon insulin stimulation following serum starvation. In nonstressed cells, no significant difference between MEFs transfected with HA-ATF(N) and the vector control was observed. ER stress induced by tunicamycin treatment severely impaired insulin signaling in the control cells (82%, $P = 0.0003$) (Fig. 8*B*). However, in tunicamycin-treated cells, ATF6(N) overexpression showed significant improvement in insulin sensitivity (3.3-fold, $P = 0.01$) compared with the vector-transfected cells (Fig. 8*B*). These in vitro experiments support our in vivo observations that adaptive UPR triggered by *Grp78* heterozygosity might contribute to the improved insulin sensitivity under HFD-induced ER stress.

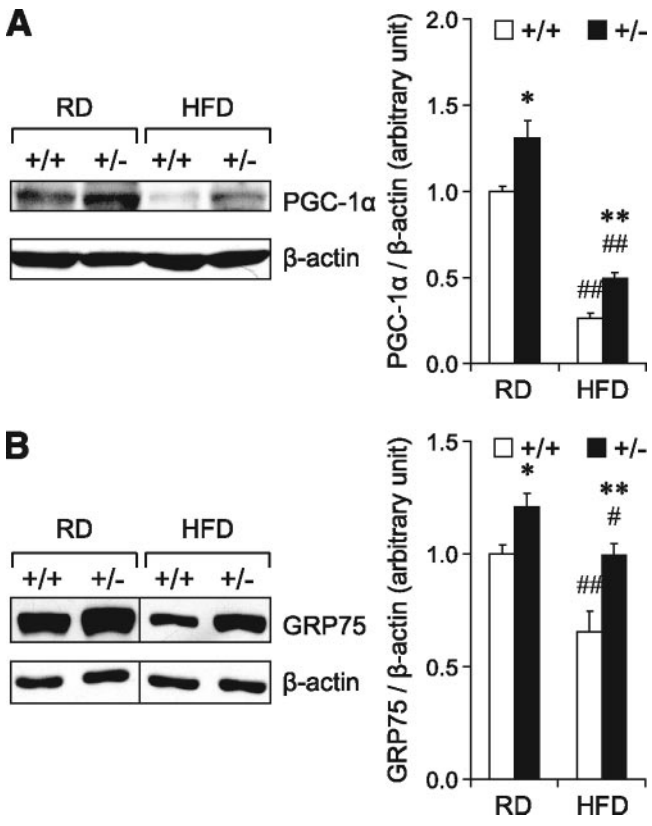

FIG. 7. *Grp78* heterozygosity upregulates PGC-1α and GRP75 in WAT. Whole cell lysates from WAT of 25-week-old mice on regular diet (RD) or after 15-week HFD ($n = 4–6$ mice per condition) were subjected to Western blotting for PGC-1α (*A*) and GRP75 (*B*). In the representative blots, lanes that were run on the same gel but noncontiguous are divided by lines. Quantitative protein levels are presented as the means ± SE. *$P < 0.05$; **$P < 0.01$ for $^{+/-}$ vs. $^{+/+}$; #$P < 0.05$; ##$P < 0.01$ for HFD vs. regular diet. □, $^{+/+}$; ■, $^{+/-}$.

DISCUSSION

While the role of ER stress in energy balance and metabolic homeostasis is still emerging, the notion that adaptive UPR may confer beneficial effects is supported by the discovery that expression of metabolic gene network is directly responsive to ER homeostasis (26). ER chaperones could also be important for energy and metabolic homeostasis. Homozygous knockout of CRT in mice leads to postnatal growth retardation, hypoglycemia, and increased levels of serum triglycerides and cholesterol (29). CRT and CNX modulate insulin signaling through association and stabilization of the insulin receptor (30,31). Thus, ER chaperones, either individually or collectively, may be protective against metabolic stress, consistent with the finding that chemical chaperones that modulate ER stress and increase ER folding capacity improve systemic insulin action (8). Here, we demonstrate that *Grp78* heterozygosity triggers adaptive UPR, resulting in attenuation of translational block, increase in GRP94 and PDI, and improvement of insulin sensitivity, particularly in WAT. Recent studies reported that the chemical chaperone 4-phenylbutyrate, in its role as modulator of the UPR, reduces weight gain in HFD-fed C57BL/6 mice by inhibiting adipogenesis (32). This provides a potential mechanism whereby improvement of ER homeostasis could result in reduced obesity. We observed that HFD led to increase in adipocyte size in both *Grp78*$^{+/+}$ and $^{+/-}$ mice and there is no apparent difference in adipocyte size or

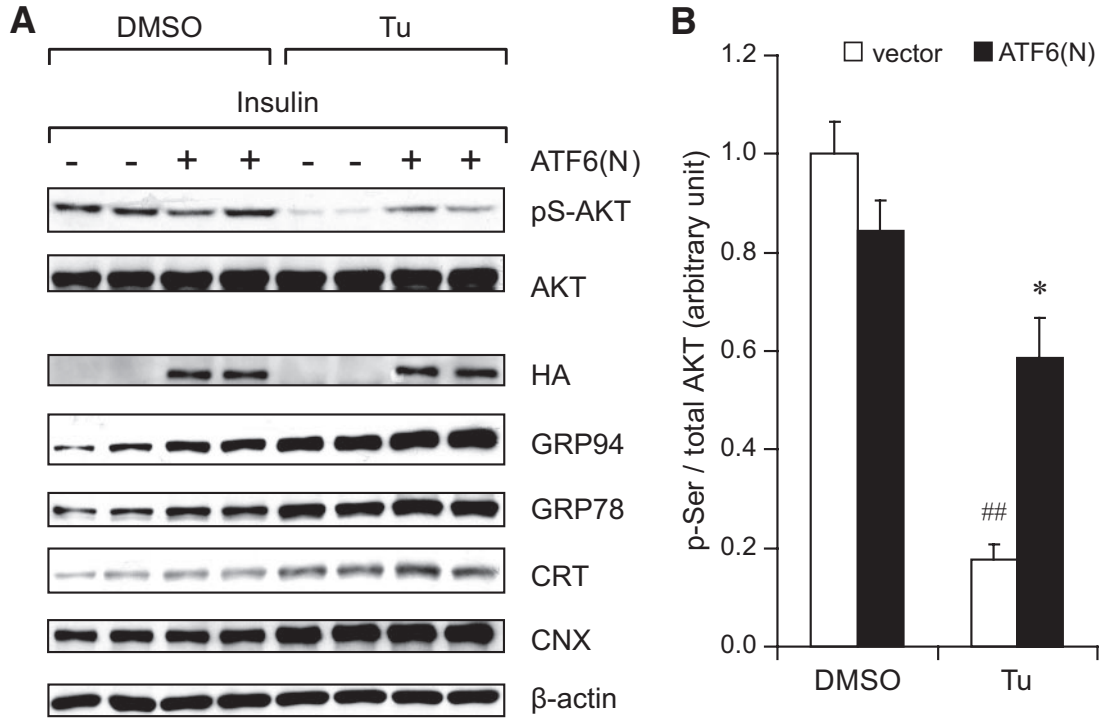

FIG. 8. Overexpression of active ATF6 improves insulin sensitivity in MEFs under ER stress. A HA-tagged nuclear form of ATF6 [ATF6(N)] was overexpressed in immortalized wild-type MEFs via transient transfection 72 h prior to insulin stimulation, controlled by the empty vector. Transfected MEFs were treated with tunicamycin (Tu, 1.5 μg/ml) or DMSO for 14 h before insulin stimulation. Following 5 h serum starvation, cells were treated with insulin (100 nmol/l, 15 min). *A*: Whole cell lysates were immunoblotted for indicated proteins. *B*: Quantitation of AKT Ser473 phosphorylation is presented as the means ± SE. **P* < 0.05 for $^{+/-}$ vs. $^{+/+}$; ##*P* < 0.01 for HFD vs. regular diet. □, vector; ■, ATF6(N).

morphology between the two genotypes, either regular diet fed or HFD fed. Nonetheless, CHOP, a known inhibitor of C/EBPα critical for adipogenesis (33), is induced in the WAT of *Grp78*$^{+/-}$ mice. This, coupled with decreased fat mass, suggests that adipogenesis might be inhibited in *Grp78*$^{+/-}$ mice via CHOP induction in preadipocytes. However, these remain to be established in future experiments. ER stress also contributes to the activation of inflammatory response and insulin/leptin resistance in hypothalamus, which could be part of the underlying mechanism of diet-induced obesity (34). Whether *Grp78* heterozygosity improves ER homeostasis in hypothalamic neurons and protects against HFD-induced obesity awaits further investigation.

In summary, while the mechanisms for observed phenotypes of the *Grp78*$^{+/-}$ mice are likely to be complex and involve multiple pathways that await further investigations, based on our results, we propose a working model as part of the contributing factors for the attenuation of diet-induced obesity and insulin resistance for the *Grp78*$^{+/-}$ mice (supplementary Fig. 7). We speculate that because of the critical requirement of GRP78 in maintaining ER homeostasis and the extra demand for protein synthesis and trafficking in the ER of WAT magnified by exposure to HFD, compensatory adaptive responses are activated, including upregulation of ER chaperones and ERAD, which improves ER homeostasis and attenuates inflammation, consequentially improving insulin signaling and glucose metabolism. The other beneficial effects from the improved ER homeostasis may include increases in mitochondrial activity and energy expenditure. These effects of *Grp78* heterozygosity mediate, in part, the resistance to diet-induced obesity, insulin resistance, and type 2 diabetes. Our studies also suggest that how UPR pathways are regulated in vivo in specific tissues under physiologic stress is likely to be more complex than what has been reported for tissue culture cells treated with pharmacological reagents. Thus, in adipose tissues subjected to diet-induced metabolic stress, we observed sustained eIF2α phosphorylation in the WAT of the HFD-fed *Grp78*$^{+/+}$ mice, correlating with translational block and downregulation of UPR markers. In contrast, eIF2α phosphorylation was much reduced in the WAT of *Grp78*$^{+/-}$ mice, consistent with upregulation of UPR markers from resumption of protein synthesis following feedback inhibition of eIF2α phosphorylation by GADD34. It is also possible that other yet unknown pathways may contribute to their upregulation.

Recently, it has been reported that GRP78 overexpression inhibits insulin and ER stress–induced sterol regulatory element–binding protein-1c activation and reduces hepatic steatosis in the *ob/ob* mice (35). These new findings support the notion that chaperone balance modulates insulin sensitivity. In their study, increase in chaperone activity is achieved through adenoviral GRP78 injection into mice; in our study, *Grp78* heterozygosity results in compensatory increase of GRP94 and PDI, as well as other adaptive UPRs. Their finding that GRP78 overexpression attenuates hepatic insulin resistance is in agreement with our observation of improved insulin signaling in MEFs, where GRP78 and other ER chaperone levels were elevated upon overexpression of active ATF6.

Potential exciting links between mitochondria function and energy expenditure to chaperone proteins have recently been reported. One explanation why GRP78 level might affect energy expenditure may lie in its property as

an ER Ca^{2+} binding protein. Partial reduction in GRP78 level could lead to increased Ca^{2+} efflux from the ER to the cytosol. Modulation of cytosolic Ca^{2+} levels has been reported to affect energy metabolism (36). There is evidence that the members of the GRP family are important regulators of mitochondria function. For instance, GRP94, which is upregulated by *Grp78* heterozygosity, is reported to molecularly interact with GRP75, an essential mitochondrial chaperone that imports mitochondrial proteins into the matrix (37). GRP75 is in turn physically linked to the voltage-dependent anion channel and mediates the coupling of ER and mitochondrial Ca^{2+} channels (28). Our studies revealed that the level of GRP75, as well as PGC-1α, is elevated in WAT of $Grp78^{+/-}$ mice. Increases in mitochondrial biogenesis and function are associated with elevated energy expenditure. We have recently discovered that in cell cultures where endogenous GRP78 was depleted by siRNA, the ER was expanded, coupled with a substantial increase in mitochondria quantity (38). In view of the emerging evidence indicating that ER and the mitochondria are linked physically and functionally at least in part through chaperone interaction, the $Grp78^{+/-}$ mouse model will provide a novel experimental system for future investigations into this exciting new area. Furthermore, with the recent establishment of the floxed *Grp78* mouse model (39), future creation of tissue-specific deletion of GRP78 will identify directly the target tissues of GRP78 function in metabolic diseases.

ACKNOWLEDGMENTS

This work is supported in part by National Institutes of Health (NIH) Grants CA027607, DK070582, and DK079999 to A.S.L.; NIH Grant TDK80756 to J.K.K.; American Diabetes Association Grants 1-04-RA-47 and 7-07-RA-80 to J.K.K.; and the Pennsylvania Department of Health Tobacco Settlement Funds to J.K.K.

No potential conflicts of interest relevant to this article were reported.

We thank Drs. Richard Bergman and Hooman Allayee and members of the Lee lab for helpful discussions and the Bergman lab for assistance on insulin ELISA. We thank Dr. Stanley Korsmeyer for providing the SV40-immortalized wild-type MEFs. We also thank Ernesto Barron at the Cell and Tissue Imaging Core facility of the University of Southern California/Norris Comprehensive Cancer Center for technical assistance on the electron microscopy. We thank Dr. Guadalupe Sabio at Dr. Roger Davis lab (University of Massachusetts Medical School) for assistance on the JNK1 measurement.

REFERENCES

1. Kaufman RJ, Scheuner D, Schroder M, Shen X, Lee K, Liu CY, Arnold SM. The unfolded protein response in nutrient sensing and differentiation. Nat Rev Mol Cell Biol 2002;3:411–421
2. Rutkowski DT, Kaufman RJ. That which does not kill me makes me stronger: adapting to chronic ER stress. Trends Biochem Sci 2007;32:469–476
3. Ni M, Lee AS. ER chaperones in mammalian development and human diseases. FEBS Lett 2007;581:3641–3651
4. Rosen ED, Spiegelman BM. Adipocytes as regulators of energy balance and glucose homeostasis. Nature 2006;444:847–853
5. Gregor MF, Hotamisligil GS. Thematic review series: adipocyte biology. Adipocyte stress: the endoplasmic reticulum and metabolic disease J Lipid Res 2007;48:1905–1914
6. Ozcan U, Cao Q, Yilmaz E, Lee AH, Iwakoshi NN, Ozdelen E, Tuncman G, Gorgun C, Glimcher LH, Hotamisligil GS. Endoplasmic reticulum stress links obesity, insulin action, and type 2 diabetes. Science 2004;306:457–461
7. Hirosumi J, Tuncman G, Chang L, Gorgun CZ, Uysal KT, Maeda K, Karin M, Hotamisligil GS. A central role for JNK in obesity and insulin resistance. Nature 2002;420:333–336
8. Ozcan U, Yilmaz E, Ozcan L, Furuhashi M, Vaillancourt E, Smith RO, Gorgun CZ, Hotamisligil GS. Chemical chaperones reduce ER stress and restore glucose homeostasis in a mouse model of type 2 diabetes. Science 2006;313:1137–1140
9. Lee AS. The glucose-regulated proteins: stress induction and clinical applications. Trends Biochem Sci 2001;26:504–510
10. Hendershot LM. The ER function BiP is a master regulator of ER function. Mt Sinai J Med 2004;71:289–297
11. Luo S, Mao C, Lee B, Lee AS. GRP78/BiP is required for cell proliferation and protecting the inner cell mass from apoptosis during early mouse embryonic development. Mol Cell Biol 2006;26:5688–5697
12. Harding HP, Zeng H, Zhang Y, Jungries R, Chung P, Plesken H, Sabatini DD, Ron D. Diabetes mellitus and exocrine pancreatic dysfunction in $perk^{-/-}$ mice reveals a role for translational control in secretory cell survival. Mol Cell 2001;7:1153–1163
13. Kim HJ, Higashimori T, Park SY, Choi H, Dong J, Kim YJ, Noh HL, Cho YR, Cline G, Kim YB, Kim JK. Differential effects of interleukin-6 and -10 on skeletal muscle and liver insulin action in vivo. Diabetes 2004;53:1060–1067
14. Lu PD, Jousse C, Marciniak SJ, Zhang Y, Novoa I, Scheuner D, Kaufman RJ, Ron D, Harding HP. Cytoprotection by pre-emptive conditional phosphorylation of translation initiation factor 2. EMBO J 2004;23:169–179
15. Luo S, Lee AS. Requirement of the p38 MAPK signaling pathway for the induction of Grp78/BiP by azetidine stress: ATF6 as a target for stress-induced phosphorylation. Biochem J 2002;366:787–795
16. Ozcan U, Ozcan L, Yilmaz E, Duvel K, Sahin M, Manning BD, Hotamisligil GS. Loss of the tuberous sclerosis complex tumor suppressors triggers the unfolded protein response to regulate insulin signaling and apoptosis. Mol Cell 2008;29:541–551
17. Surwit RS, Kuhn CM, Cochrane C, McCubbin JA, Feinglos MN. Diet-induced type II diabetes in C57BL/6J mice. Diabetes 1988;37:1163–1167
18. Cusi K. Nonalcoholic fatty liver disease in type 2 diabetes mellitus. Curr Opin Endocrinol Diabetes Obes 2009;16:141–149
19. Wellen KE, Hotamisligil GS. Inflammation, stress, and diabetes. J Clin Invest 2005;115:1111–1119
20. Sabio G, Das M, Mora A, Zhang Z, Jun JY, Ko HJ, Barrett T, Kim JK, Davis RJ. A stress signaling pathway in adipose tissue regulates hepatic insulin resistance. Science 2008;322:1539–1543
21. Rutkowski DT, Arnold SM, Miller CN, Wu J, Li J, Gunnison KM, Mori K, Sadighi Akha AA, Raden D, Kaufman RJ. Adaptation to ER stress is mediated by differential stabilities of pro-survival and pro-apoptotic mRNAs and proteins. PLoS Biol 2006;4:e374
22. Rutkowski DT, Kaufman RJ. A trip to the ER: coping with stress. Trends Cell Biol 2004;14:20–28
23. Ma Y, Hendershot LM. Delineation of a negative feedback regulatory loop that controls protein translation during endoplasmic reticulum stress. J Biol Chem 2003;278:34864–34873
24. Novoa I, Zeng H, Harding HP, Ron D. Feedback inhibition of the unfolded protein response by GADD34-mediated dephosphorylation of eIF2alpha. J Cell Biol 2001;153:1011–1022
25. Lee AH, Iwakoshi NN, Glimcher LH. XBP-1 regulates a subset of endoplasmic reticulum resident chaperone genes in the unfolded protein response. Mol Cell Biol 2003;23:7448–7459
26. Rutkowski DT, Wu J, Back SH, Callaghan MU, Ferris SP, Iqbal J, Clark R, Miao H, Hassler JR, Fornek J, Katze MG, Hussain MM, Song B, Swathirajan J, Wang J, Yau GD, Kaufman RJ. UPR pathways combine to prevent hepatic steatosis caused by ER stress-mediated suppression of transcriptional master regulators. Dev Cell 2008;15:829–840
27. Cunningham JT, Rodgers JT, Arlow DH, Vazquez F, Mootha VK, Puigserver P. mTOR controls mitochondrial oxidative function through a YY1-PGC-1alpha transcriptional complex. Nature 2007;450:736–740
28. Szabadkai G, Bianchi K, Varnai P, De Stefani D, Wieckowski MR, Cavagna D, Nagy AI, Balla T, Rizzuto R. Chaperone-mediated coupling of endoplasmic reticulum and mitochondrial Ca2+ channels. J Cell Biol 2006;175:901–911
29. Guo L, Nakamura K, Lynch J, Opas M, Olson EN, Agellon LB, Michalak M. Cardiac-specific expression of calcineurin reverses embryonic lethality in calreticulin-deficient mouse. J Biol Chem 2002;277:50776–50779
30. Bass J, Chiu G, Argon Y, Steiner DF. Folding of insulin receptor monomers is facilitated by the molecular chaperones calnexin and calreticulin and impaired by rapid dimerization. J Cell Biol 1998;141:637–646
31. Ramos RR, Swanson AJ, Bass J. Calreticulin and Hsp90 stabilize the human

insulin receptor and promote its mobility in the endoplasmic reticulum. Proc Natl Acad Sci U S A 2007;104:10470–10475
32. Basseri S, Lhotak S, Sharma AM, Austin RC. The chemical chaperone 4-phenylbutyrate inhibits adipogenesis by modulating the unfolded protein response. J Lipid Res. 21 May 2009 [Epub ahead of print]
33. Batchvarova N, Wang XZ, Ron D. Inhibition of adipogenesis by the stress-induced protein CHOP (Gadd153). EMBO J 1995;14:4654–4661
34. Zhang X, Zhang G, Zhang H, Karin M, Bai H, Cai D. Hypothalamic IKKbeta/NF-kappaB and ER stress link overnutrition to energy imbalance and obesity. Cell 2008;135:61–73
35. Kammoun HL, Chabanon H, Hainault I, Luquet S, Magnan C, Koike T, Ferre P, Foufelle F. GRP78 expression inhibits insulin and ER stress-induced SREBP-1c activation and reduces hepatic steatosis in mice. J Clin Invest 2009;119:1201–1215
36. Chan SL, Liu D, Kyriazis GA, Bagsiyao P, Ouyang X, Mattson MP. Mitochondrial uncoupling protein-4 regulates calcium homeostasis and sensitivity to store depletion-induced apoptosis in neural cells. J Biol Chem 2006;281:37391–37403
37. Takano S, Wadhwa R, Mitsui Y, Kaul SC. Identification and characterization of molecular interactions between glucose-regulated proteins (GRPs) mortalin/GRP75/peptide-binding protein 74 (PBP74) and GRP94. Biochem J 2001;357:393–398
38. Li J, Ni M, Lee B, Barron E, Hinton DR, Lee AS. The unfolded protein response regulator GRP78/BiP is required for endoplasmic reticulum integrity and stress-induced autophagy in mammalian cells. Cell Death Differ 2008;15:1460–1471
39. Fu Y, Wey S, Wang M, Ye R, Liao CP, Roy-Burman P, Lee AS. *Pten* null prostate tumorigenesis and AKT activation are blocked by targeted knockout of the stress response chaperone GRP78/BiP in prostate epithelium. Proc Natl Acad Sci U S A 2008;105:19443–19448